Supplementary Information: Decoding ultrafast water transport in graphene oxide

Vikas Yadav,[a] Sangram Kishor Behera[a], Anjan Das[a], Chitti Venkata Krishnamurthy[a] and Manu Jaiswal*[a]

Received 00th January 20xx, Accepted 00th January 20xx DOI: 10.1039/x0xx00000x

S1: Solution-diffusion Model

Solution–diffusion is the most common process governing the permeation of gases or moisture through microporous membranes. Permeation of molecules through adsorbing pores can be described using the solution–diffusion model[1]. In this model, molecules adsorb into the membrane depending on their adsorption affinity. The permeation rate is expressed as $J = -D_k \frac{\Delta c}{\Delta x}$ Here Δc is the concentration difference of adsorbing material between the feed and permeate sides, and D is the effective transport diffusion constant of the adsorbing material. The value of concentration can be directly obtained from the sorption isotherm. One can estimate the value of the diffusion constant with loading if a small concentration gradient is maintained, such that D can be taken as constant for that interval[2–4]. The concentration c is often expressed in terms of the solubility of the adsorbing material inside the polymeric matrix. Hence, materials with lower D and low S are ideal for a moisture barrier. A combination of both diffusion and sorption results in the overall permeation rate. Materials with low water uptake capacity, such as Teflon, Kapton film, Parafilm, polyethene, polypropylene, etc, generally have a low water permeation rate.[5,6] On the other hand, materials such as PDMS and Nafion allow higher water vapour permeation. Despite having a very low water sorption capacity, the vapour permeation rate in PDMS is quite good due to a faster diffusion coefficient[7]. Where Nafion shows the highest vapour permeability due to the combination of large sorption capacity[8] and faster diffusion coefficient[9]. It is also clear that the rate of vapour permeation in GO is not exceptionally high compared to other polymers, such as Nafion membranes. Therefore, the observed high vapour permeation can be explained based on this sorption diffusion model[10,11]. as given in Table S1.

Table S1 Vapour permeation rates of materials

Materials	vapour permeation rate (Barrer)	Reference
Polyethylene	12	5
Kapton	500	6
Polysulfone	2000	6
PDMS	100000	11
GO	400000	12
Nafion 115	10000000	10

S2: Sorption Isotherm

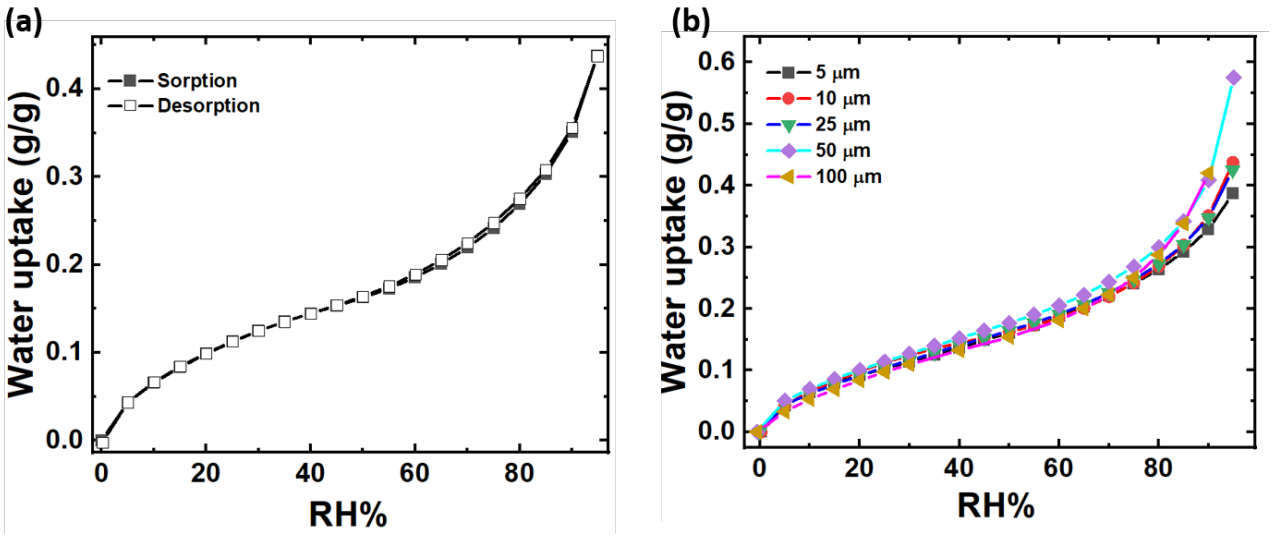

Fig. S1 (a) Sorption (filled square) and desorption (open square) of water in GO at different RH%. (b) Water sorption isotherm of GO for various thicknesses ranging from 5 to 100 μm.

S3: External mass transfer resistance

The values of open aperture permeation rate for 5% RH difference for various feed RH% are given in the Table S2. The average stagnation layer resistance R_s was nearly constant across the entire RH% interval, with $R_s = 0.056 \pm 0.004$ cm^2 min./μg.

Table S2 Evaporation rate of water from saturated salt solution in permeation cell under 5% RH difference.

Salt solution	RH%	ΔRH	permeation rate(μg/min.cm^2)	R$_s$(cm^2 min./μg)
LiCl	11%	5%	17.4	0.057
$Mg(NO_3)_2$	54%	5%	16.2	0.061
NaCl	75%	5%	19.2	0.052
KCl	84%	5%	18.6	0.053
Pure Water	100%	5%	17.4	0.057

S3.1: COMSOL modelling

We also performed COMSOL modelling of the air/solid phase convection/diffusion to examine the presence of a stagnation layer. A 2D axisymmetric geometry was employed, using the 'Laminar Flow'and 'Transport of Dilute Species'modules. The cylindrical geometry of the sorption chamber, with a height of 90 mm and a diameter of 50 mm, was implemented in the model. The dimensions and geometry of the permeation cell were measured and used for COMSOL simulations. Nitrogen gas was chosen as the medium with 250 sccm flow at 25 °C and the diffusion coefficient of water in the gas phase was set to be 2.5 × 10^{-5} m^2/s. The air just above the solution was assumed to be governed by pure water (100% RH near its surface) or the RH of the saturated salt solution, while the permeate side humidity was set at 5% RH lower than the feed-side value.

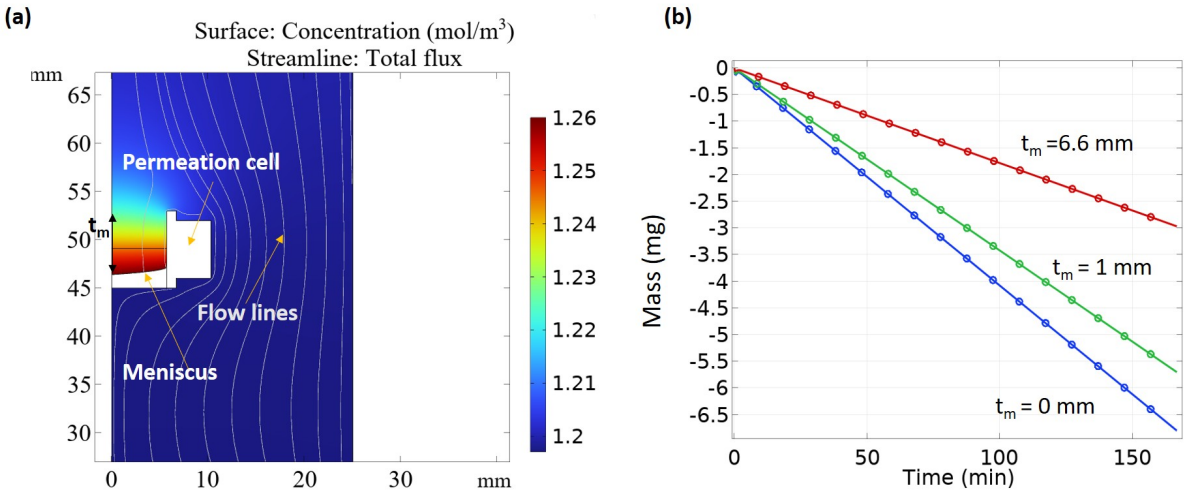

Fig. S2 (a) Simulated concentration profile of water vapour from evaporating water meniscus under 250 sccm flow of 95% RH. The colour scale bar represents the concentration of water vapour in the gas phase. (b) Mass loss with time through open aperture for different meniscus positions, t_m, measured from the top of the permeation cell.

Fig. S2(a) presents the cross-sectional view of the geometry, showing the flow-lines of water vapour loaded N_2 at steady state. A gradient of water vapour concentration is observed just above the meniscus, which acts as a stagnant layer. The permeation rate can be calculated from the gradient of water vapour concentration and diffusion constant as $J = -D_w^g \frac{dC}{dx}$ along the vertical direction. Here, t$_m$ is the depth of the meniscus from the top of the permeation cell or the level of filling of the solution as shown in Fig. S2(a). We have introduced this to see the effect of liquid filling on the open aperture permeation rates. Fig. S2(b) presents the mass loss with time for three different t$_m$ values, revealing a significant effect of meniscus position on the open aperture permeation rate. The table provides the values of permeation rates calculated from COMSOL modelling at different values of t$_m$ along with experimentally observed values.

Table S3 Validation of the COMSOL simulations.

t$_m$ (mm)	Permeation rate(μg/min.cm^2) Experiment	Permeation rate(μg/min.cm^2) COMSOL
6.6	17.7	17.4
1	35	33.5
0	44	42

The above comparison was used to validate the COMSOL model. Thus, the results from COMSOL modelling can be used to identify the stagnation layer contribution. The value of permeation rate for open aperture for 100% RH difference in our case was observed to

be around 2 times smaller than the value reported by Nair et al.,[12], likely due to differences in liquid level in the cell, and our simulation result can explain this deviation.
The values obtained from modelling and experiment are in close agreement. All our permeation experiments with film were conducted for t_m= 6.6 mm. The obtained value from COMSOL modelling was 17.4 μg/min.cm^2, which is in fair agreement with the mean value from the experimental data (17.7 μg/min.cm^2). Therefore, we have used the stagnation layer resistance value around 0.057 cm^2 min./μg to obtain the correct permeation resistance through the membrane.

S4: Sorption experiments

The sorption time constant (τ) was found to increase linearly with the membrane thickness (see Figure S3(a))[13]. This behaviour is typically observed in cases where the sorption process is limited by the external mass transfer process, as given by the relation below[13]:

$$\tau \propto \Gamma_{dry} K$$

The proportionality constant depends upon the external mass transfer resistance (stagnation layer thickness). Here, Γ_{dry} is the mass per unit area of the GO membrane 'seen'by the water molecules, and in our case, planar geometry, this is proportional to the thickness of the membrane. The factor K is related to the water uptake capacity of the membrane in the RH% interval, which can be obtained from sorption isotherm values.

$$K = \frac{\Delta(M/M_{dry}) \times 100}{\Delta RH\%}$$

Since the external mass transfer resistance depends on the flow rate, sorption kinetics measurements were performed at different carrier gas flow rates, which verifies this effect (Figure S3(b)).

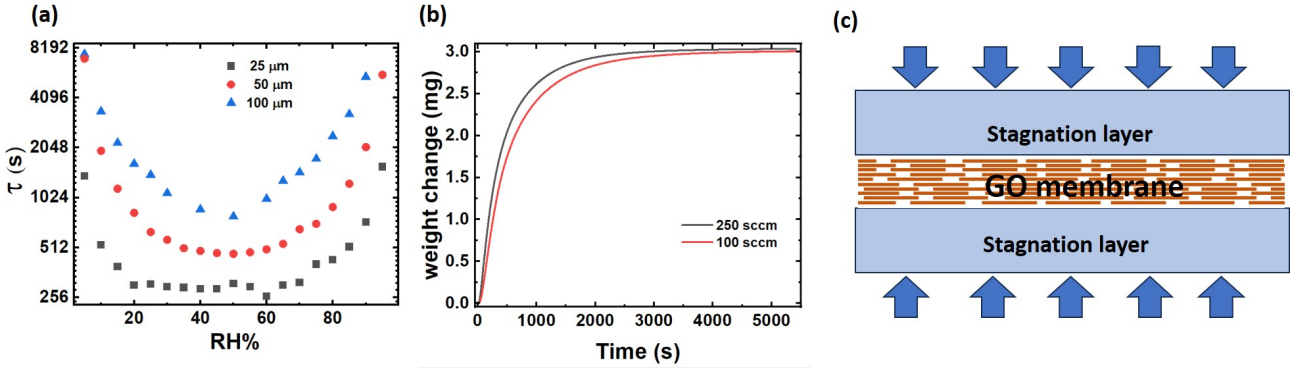

Fig. S3 (a) Calculated water sorption time constant for GO with three different thicknesses 25 μm, 50 μm and 100 μm in the GO membrane with a thickness at various RH%. (b) Sorption kinetics of water for two carrier gas flow rates, 100 sccm and 250 sccm. (c) Schematic cross-section of a stacked flakes GO membrane for out-plane water sorption, showing stagnation layers on both surfaces of the membrane.

Therefore, Fig. S3(c) provides a better schematic representation of the water sorption, including external mass transfer resistance described as a stagnation layer.

S4.1: Internal vs. external mass transfer rates

To evaluate whether the transport is limited by external or internal resistance, the Biot number is commonly used as a diagnostic parameter[14]. It is an indicator of internal to external mass transfer rates, which not only depend on the length, diffusion coefficient, and external mass transfer, but also on the sorption capacity at given RH%.

$$\mathrm{B_i} = \frac{k_e l \Delta c^v}{D \Delta C_m}$$

Here, k_e is the external mass transfer coefficient, which can be defined in terms of external mass transfer resistance as $R_{ss}=\frac{1}{Ak_e}$ and A is the area of membrane in contact with the gas phase.
D is the effective diffusion constant of water inside the material, l is the half thickness of the membrane, and $\frac{\Delta C_m}{\Delta C^v}$ is the concentration of adsorbed water in the membrane per unit change in the concentration of water vapour in the air phase[14].
$B_i >> 1$ indicates an internal diffusion-limited process.
$B_i \approx 1$ indicates that both external and internal diffusion are contributing significantly.
$B_i << 1$ indicates external diffusion-limited process.

S4.2: Estimation of external mass transfer coefficient

The analytical estimation of this external mass transfer coefficient is made using the Sherwood number[15,16].

$$Sh = \frac{\kappa_e}{D}$$

κ_e: mass transfer coefficient (m/s)
D: diffusion coefficient (m^2/s)
For a planar sample of length L, the average Sherwood number

$$\overline{Sh} = 0.664 Re^{1/2} Sc^{1/3}$$

Here, $Re = \frac{u_\infty L}{\nu}$ is Reynolds number. and $Sc = \frac{\nu}{D}$ is Schmidt number and carrier gas parameters ν is kinematic viscosity and u_∞ is free-stream velocity.
For a 250 sccm flow through a 50 mm diameter (chamber diameter), the average velocity would be around $u_\infty \sim 2.2 \times 10^{-3}$ m/s, giving a value of $\kappa_e = 1.2 \times 10^{-3}$ m/s. This value is in a similar order to the value reported in the literature[13,14].

S4.3: Experimental estimation of the external mass transfer coefficient

To estimate the external mass transfer coefficient for sorption measurements, we used the wet cloth method, similar to that described in the literature[14]. The mass transfer coefficients were calculated from the water evaporation rate (without accounting for temperature effects). Based on the above calculations, the thickness of the stagnation layer was estimated to be around 14 ± 1 mm. The corresponding external mass transfer coefficient is around 1.8 $\times 10^{-3}$ m/s ($\delta = 14$mm). which is comparable to the value estimated using the Sherwood formula.
Alternative estimations of the external mass transfer coefficient can be obtained from numerical or fluid dynamic simulations. Apart from these analytical expressions and simulation studies, direct measurement of the external mass transfer coefficient is obtained by drying kinetics of a wet surface under a controlled environment. Our simulation study performed in COMSOL yielded an average external mass transfer coefficient of approximately 2.1 $\times$ 10^{-3} m/s ($\delta = 12$mm), which is in close agreement with the obtained experimental value. We considered the experimentally obtained values of the stagnation layer thickness to obtain the robust estimates of the out-of-plane diffusion coefficient of water molecules in the GO membrane.

S4.4: Correcting the D value

The thickness of the stagnation layer (or external mass transfer coefficient) was obtained as described above. This was used as an input for the COMSOL simulations. The following boundary conditions were imposed:
(1) At the stagnation layer/membrane interfaces:
(a) Flux at the interface

$$J_{in} = D_w^g \nabla c_v$$

Here, ∇c_v is the concentration gradient of water molecules in the gas phase at the interface.
(b) Concentration of water at the interfaces

$$C = S_m c_v / S_0$$

(2) At the stagnation layer boundary:
At $t = 0$,

$$c^v = C^v_{RH1}$$

For $t > 0$,

$$c^v = c^v_{RH2}(1 - e^{(-t/\tau_{RH})})$$

Here, τ_{RH} is the characteristic time for setting RH%. We measured this time (τ_{RH}) to be around 80 s.
The simulation gives the temporal evolution of the mass loading kinetic curve, and the sorption time constant was estimated from this curve from the time to achieve 63% of the saturation value. The value of this time constant depends on the value of stagnation layer thickness, diffusion coefficient for water molecules, material properties, membrane thickness, and the water uptake by the material in the ΔRH% (RH_2-RH_1)[13]. The sorption isotherm of the GO membrane provides the water uptake at all the RH% points. Therefore, except for the diffusion constant, the value of all the other parameters, such as stagnation layer thickness ($\delta = 14$ mm), membrane thickness, and uptake capacity, are known. Fig. S4(a) presents the effect of the diffusion coefficient of water molecules in the GO membrane (100 μm) on τ through COMSOL simulations for a 5% RH step (60% to 65% RH). For D $> 10^{-11}$ m^2/s, the sorption time is almost constant, representing external mass transfer limited sorption kinetics (light red shaded interval), τ_{stag}. The corresponding Biot numbers are also plotted on the right ordinate. The experimentally determined sorption time, τ_{exp}, is marked with a star, with an associated Biot number of 0.73. This suggests that even for 100 μm thick film, diffusion is predominantly controlled by mass transfer through the stagnation layer. Although the Biot number is smaller than 1, there is 40% increase in τ_{exp} (1295 s) in comparison to τ_{stag} (930 s), indicating the contribution of diffusion through the membrane in the sorption kinetics. By adjusting the diffusion coefficient in the simulation until τ_{sim} matches τ_{exp}, the diffusion coefficient of water for out-of-plane geometry (D^s_{out}) can be determined, as shown in Fig. S4(b). The procedure described above was applied at each RH% sorption step.

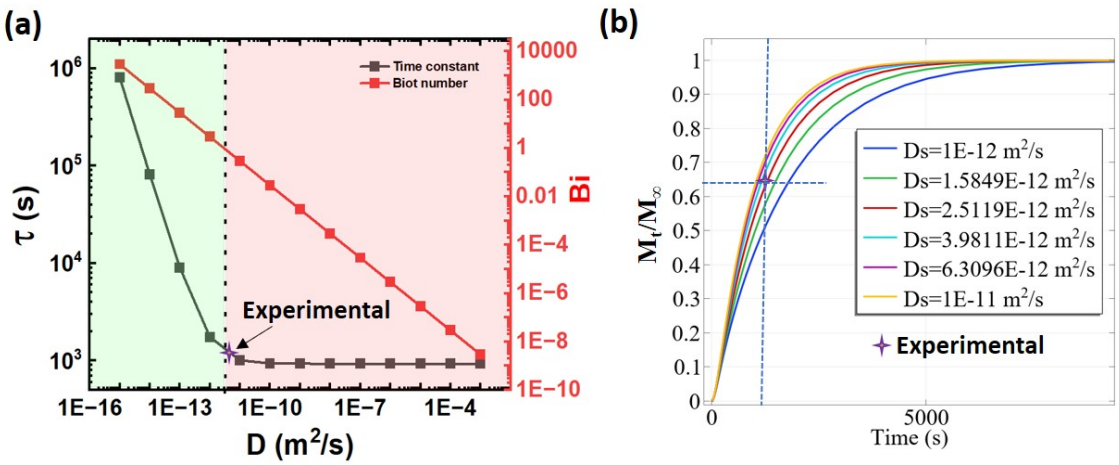

Fig. S4 (a) Simulated sorption time for a 100 μm GO membrane by varying the internal diffusion coefficient from 10^{-15} to 10^{-3} m^2/s. The stagnation layer thickness is taken as 14 mm. The Biot number is shown on the right ordinate. Regions dominated by internal kinetics are shaded light green, while the external mass transfer-limited sorption kinetics interval is shaded light red. (b) Simulated sorption curves for various internal diffusion values, to estimate the diffusion coefficient value matching the experimental sorption time. Here, the symbol, D_s, represents the diffusion of molecules within the membrane. (c) Estimated out-of-plane geometry diffusion coefficient with RH% from sorption and permeation experiments. The error bars for each data point in the diffusion coefficient from the sorption experiment represent the propagated uncertainty arising from the estimated stagnation layer thickness.

S5: Flake-size effects

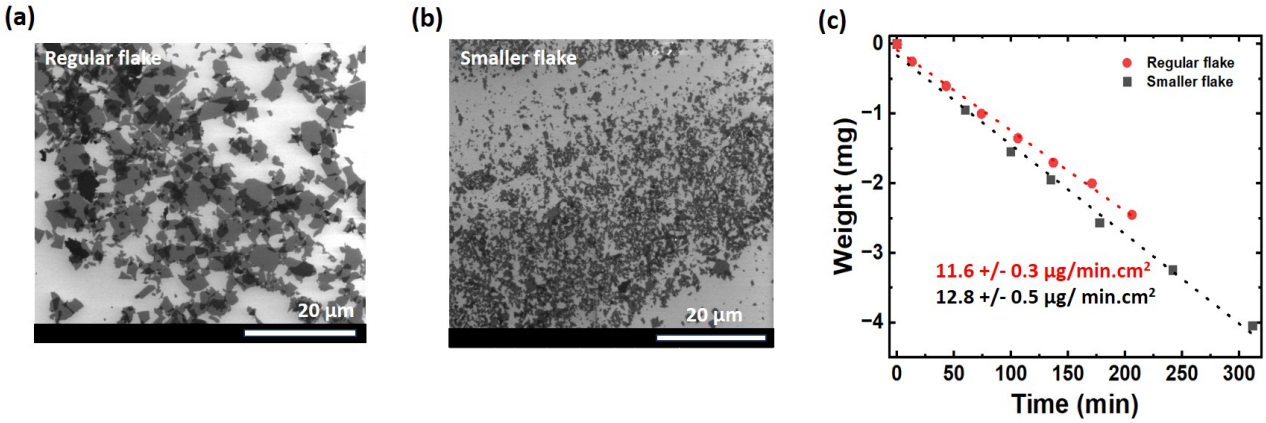

Fig. S5 (a) FESEM image of as-purchased GO flakes cast on SiO_2/Si substrate from a dilute dispersion. (b) GO flakes cast after 10 h sonication. The scale bar in both images is 20μm. (c) Water weight loss through the small flake-size GO membrane (black) in comparison to loss through the regular flake-size GO membrane for a 5% RH gradient with 54% RH on the feed side.

The size of GO flakes was decreased by a factor of 5 by ultrasonication of the aqueous dispersion. Fig. S5(a) and (b) present the FESEM images of regular flake-size and small flake-size GO obtained after sonication. GO membrane (50 μm thick) with a small flake size was prepared using vacuum filtration. Next, the vapour permeation rate through this membrane was examined using the modified permeation cell, allowing for a direct comparison of the results without the influence of stagnation layer effects. Fig. S5(c) presents the water weight loss (water) through 50μm GO membranes with regular and small flake sizes.

S6: In-plane sorption measurements

GO membrane samples were sandwiched between two moisture-impermeable layers using a suitable adhesive to ensure a sealed system, shown by the schematic in Fig. S11(a). This geometry restricts through-plane (out-of-plane) moisture flow, and thereby, transport occurs only along the planes of sheets.

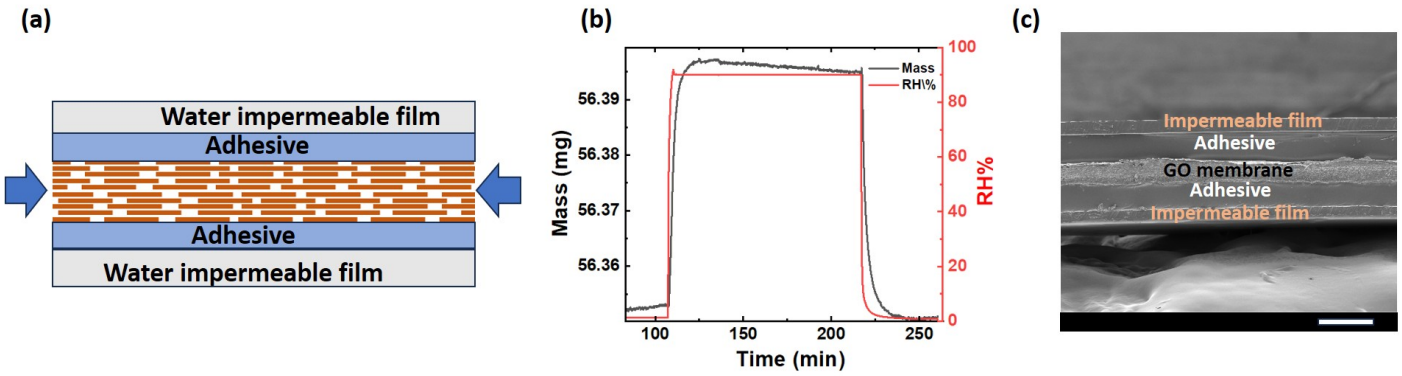

Fig. S6 (a) Schematic of GO membrane sandwiched between two moisture barrier films using an adhesive. (b) Water sorption by PDMS at room temperature, from 0% to 90% RH. (c) Cross-sectional FESEM image of sandwiched GO membrane, scale bar 100μm

To choose a moisture impermeable membrane, we checked the permeation rate of water through various materials with the feed-side maintained at 100% RH and the permeate side maintained at ambient humidity (40% RH). These experiments were performed outside the DVS instrument, and the obtained permeation rates are provided in Table S10. The above data suggest that both aluminium foil

Table S4 Permeation rate of water vapour through different materials with feed-side at 100% RH and permeate-side at 40% RH

Membrane	thickness (μm)	Permeation rate (μg/cm^{2}min)
PDMS	50	31
Kapton	25	4.2
Cling film	10	9.6
Aluminium foil	11	~0.1
Parafilm	127	~0.1
PDMS-GO-PDMS	10-10-10	84

and Parafilm can serve as effective moisture-impermeable membranes. However, due to Parafilm's poor adhesive properties, we selected aluminium foil for our studies. Next, we considered adhesive materials for interfacing the aluminium foil with the GO membrane. Here, we considered three candidates: Stycast 1266, Araldite, and PDMS. The adhesive is required to have minimal water uptake so that the membrane's sorption kinetics and sorption time estimates are not affected. Fig. S11(b) presents the mass change in PDMS from water uptake due to a change in RH from 0% to 90%. The mass change is only 40 μg, for 56 mg dry mass of PDMS, which is comparable to the empty sample holder mass change (50 μg). These results indicate negligible water sorption capacity by PDMS, ensuring it does not contribute significantly to the sorption measurements. We also tested Stycast 1266 and Araldite, but the water sorption capacity was more than 1% (g/g). Therefore, we used PDMS as the adhesive due to its extremely low water sorption and its non-reactivity with the GO membrane. Fig. S11(c) presents the cross-sectional FESEM image of the sandwiched GO membrane between two aluminium foil sheets, acting as moisture barrier layers. We did not find any visible gap at the interfaces between the GO-adhesive and the adhesive foils.

S6.1: Restriction on swelling

Prior to the sorption experiments, we performed additional tests, including RH-dependent thickness measurements and XRD analysis, to verify that the GO membrane retains its swelling capability in the sandwiched configuration. Fig. S7 presents the cross-sectional images of bare and sandwiched GO membranes in a controlled humidity environment under an optical microscope. The extent of swelling was found to be similar in both cases. The thickness of the bare and sandwiched membranes at different RH is given in the Table S5. Additionally, we prepared a separate set of GO membranes sandwiched between Kapton films to verify the swelling behaviour using X-ray diffraction (XRD) at three humidities. Fig. S8(a) and (b) present X-ray diffraction peaks for the bare and sandwiched GO membrane at three humidities. The observed shifting of the (001) peak confirms intercalation of water, indicating humidity-induced swelling in the sandwich membrane. Table S7 presents the equilibrium interlayer spacing at three different RH% for the bare and sandwiched membranes. The interlayer spacing in both cases remains nearly identical across all humidity conditions, confirming that the sandwiched membrane undergoes comparable microscopic swelling.

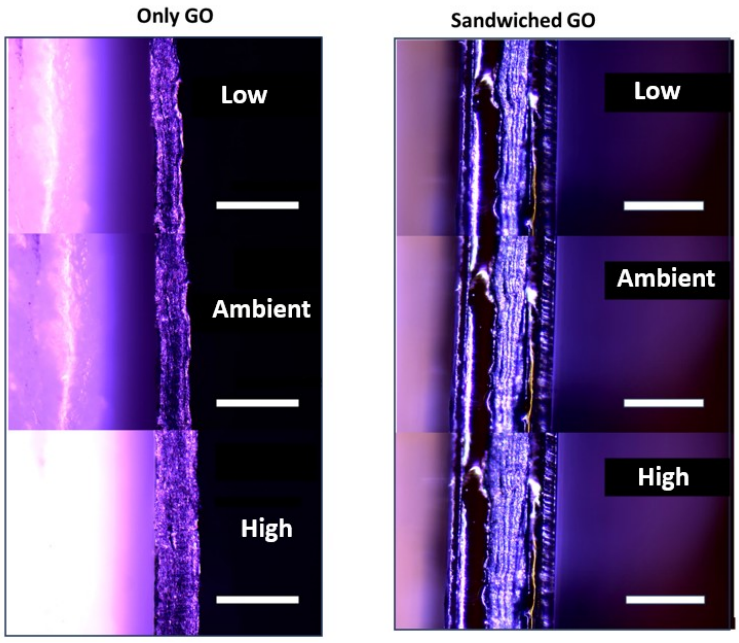

Fig. S7 Thickness of bare and sandwiched GO membranes under low (∼10% RH), ambient (∼50% RH), and high RH% (∼90% RH) measured under optical microscope. The scale bar in all images is 100μm.

Table S5 Thickness of bare and sandwiched GO membranes under different RH conditions.

RH%	bare GO thickness (μm)	sandwiched GO thickness (μm)
Low RH	32 $\pm$ 2	31 $\pm$ 2
Ambient RH	37 $\pm$ 2	36 $\pm$ 2
High RH	52 $\pm$ 2	49 $\pm$ 2

Table S6 Interlayer spacing of bare and sandwiched GO membranes at three RH levels

RH%	bare GO d-spacing (Å)	sandwiched GO d-spacing (Å)
2	7.1	7.2
45	8.3	8.2
100	12.6	12.3

Both macroscopic (thickness) as well as microscopic (interlayer spacing) results showed that the degree of swelling in the sandwiched geometry was identical to that of the bare GO membrane, confirming that the membrane undergoes comparable microscopic swelling under both conditions.

S6.2: Contribution of external mass transfer resistance

Similar to the out-plane geometry case, there could be a significant contribution from the stagnation layer for the sandwiched geometry. To understand the effect of aperture size on the stagnation layer, we conducted evaporation experiments and COMSOL simulations with smaller aperture sizes. Fig. S9 shows a COMSOL simulation presenting the effect of aperture size on the vapour concentration of water near the aperture. Spatial spread of the concentration increases for a larger aperture, resulting in an effective slower permeation of molecules through the larger aperture. Area-normalised permeation rates are also given inside the figure. To confirm the effect of aperture area, we conducted permeation experiments using aluminium foil with a small aperture to allow vapour permeation through it. For this study, 2 types of apertures were used: circular/square apertures and slit-like apertures, as shown in Fig. S10. The slit-like pore was chosen to mimic the cross-sectional aperture of the GO membrane in sandwiched geometry.

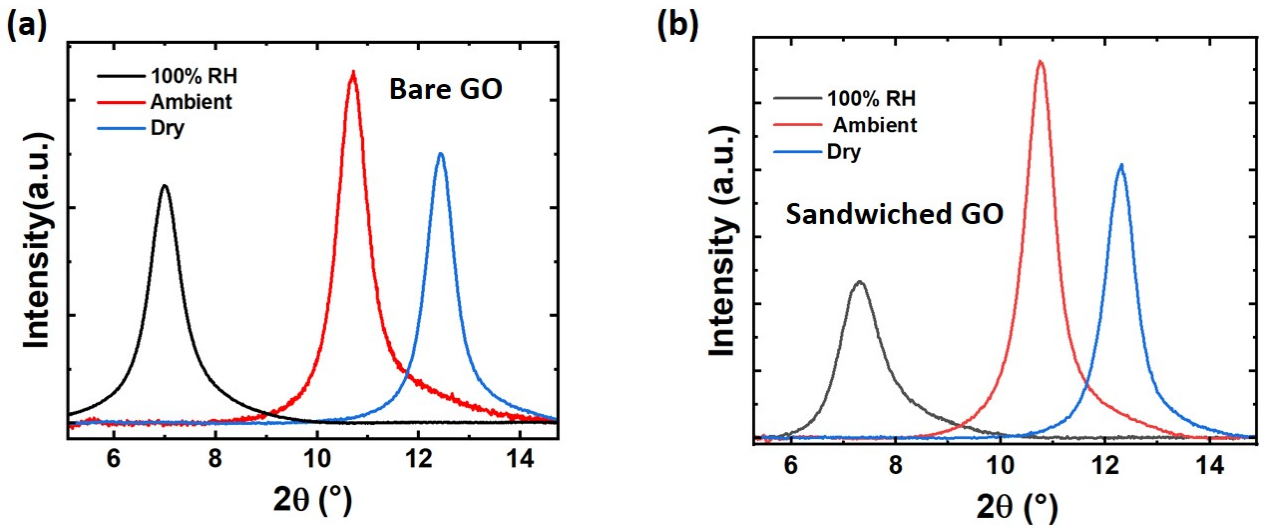

Fig. S8 XRD of (a) bare GO membrane and (b) sandwiched GO membrane at 2% RH (dry), 45% RH (ambient), and 100% RH.

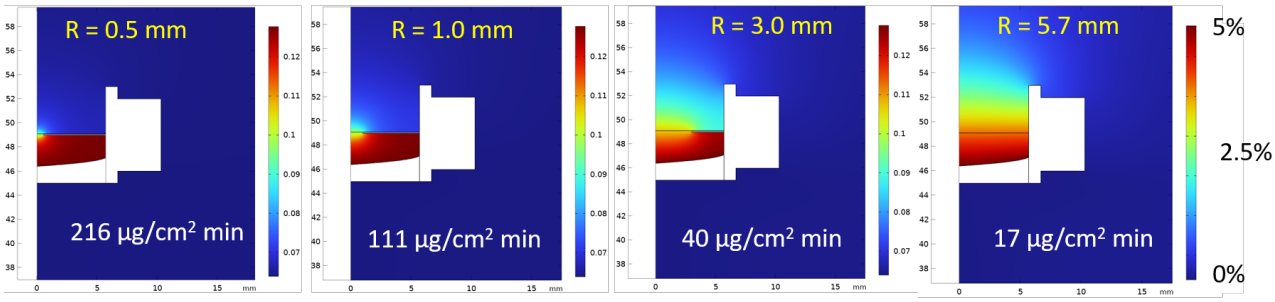

Fig. S9 Simulated vapour concentration through permeation cell with aperture diameter size: (a) 1 mm, (b) 2 mm, (c) 6 mm, and (d) 11.4 mm for 5% RH gradient. The colour chart on the right side shows the RH% relative to the chamber RH%.

The simulations and experimentally observed permeation rates through different-sized and shaped apertures are given in Table S7. Both experimental and simulation studies consistently demonstrate that the size and shape of an aperture significantly influence the evaporation rate. Notably, both approaches reveal that as the aperture size decreases, the area-normalised evaporation flux increases. Apart from the size of the aperture, the geometry of the aperture is also an important consideration. For instance, the area-normalised permeation rate is higher for a slit-shaped aperture as compared to a circular aperture.

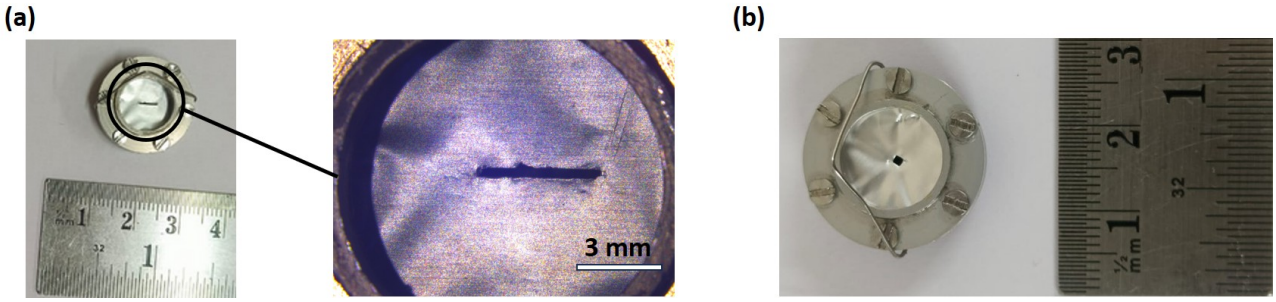

Fig. S10 Digital pictures of (a) slit-like aperture, (b) circular aperture in aluminium foils.

Both experiments and simulations confirmed the formation of a thinner stagnation layer for a smaller aperture, such as in the case of in-plane geometry. Based on our COMSOL simulation studies, the thickness of the stagnation layer for sorption measurement in the in-plane geometry is estimated to be around 0.2 mm, which is almost two orders of magnitude smaller than the measured value for out-of-plane sorption (14 mm).

For in-plane sorption studies, a 100 μm thick GO membrane sandwiched between aluminium sheets was cut into a 2.6 mm wide and 10 mm long rectangular shape. Considering a 0.2 mm stagnation layer and an average value of sorption capacity around 0.003 (g/g) per RH%, the Biot number for this geometry would be more than 1 for D $< 10^{-8}$ m^2/s. This implies that, under those diffusion coefficients,

Table S7 Experimental and simulated permeation rates of water vapour through apertures of different sizes and shapes

Aperture size	area	permeation rate	Permeation rate
	(mm^2)	(experimental)	(simulation)
		$\mu g/cm^2 min$	$\mu g/cm^2 min$
11.3 mm circular	100	17.7	17.4
1 mm square	1	175	
4.4 mm × 0.35 mm slit	1.5	220	
3 mm × 0.2 mm slit	0.6	333	
1 mm circle	0.8		216
1.1 mm circle	1		180
2 mm circle	3.1		111
6 mm circle	28.3		40
10 mm × 0.1 mm sandwiched disc	0.82		850

internal mass-transfer resistance is comparable to or greater than external resistance. Further, the experimentally inferred time constants were much larger than the characteristic time associated with the stagnation layer ($\tau_{exp}/\tau_{stag}>>1$), indicating that sorption kinetics are dominated by internal diffusion rather than by the external stagnation layer.

S6.3: Effect of adhesive

Although PDMS has a very low water sorption capacity, it exhibits relatively high water vapour permeability. As a result, there could potentially be a contribution of moisture transport through the PDMS layer to the GO membrane, as illustrated in the schematic Fig.S11(a). And S11(b) shows the cross-sectional FESEM image of a representative GO membrane sample used for the sorption kinetics study. The contribution of the water flux through PDMS and GO is represented by symbols P and G, respectively. To understand the contribution of flux through PDMS, we performed COMSOL simulations. The value of the diffusion coefficient of water molecules inside PDMS was calculated from the vapour permeation rate, Table S10, and the sorption capacity using the solution-diffusion model. The calculated value of the diffusion coefficient of water inside PDMS turns out to be around 1×10^{-9} m^2/s. This is consistent with values reported in the literature[17]. We investigated the contributions of water sorption kinetics in GO (100 μm) originating from the PDMS layer (50μm thickness on both sides). For this, vapour sorption was allowed exclusively through the PDMS cross-section, while in-plane diffusion within GO was restricted. Therefore, water molecules could only be transferred to GO across the PDMS–GO interface, taking into account the out-of-plane diffusion constant of GO determined from previous experiments. Table S8 provides the simulated sorption times for the sandwiched sample for the case when sorption by GO is only allowed through PDMS, and a comparison of the sorption time obtained from experiments. It can be seen that in all the cases, experimentally obtained time is an order of magnitude lower in comparison to the time it would have taken if the water sorption were allowed only through PDMS.

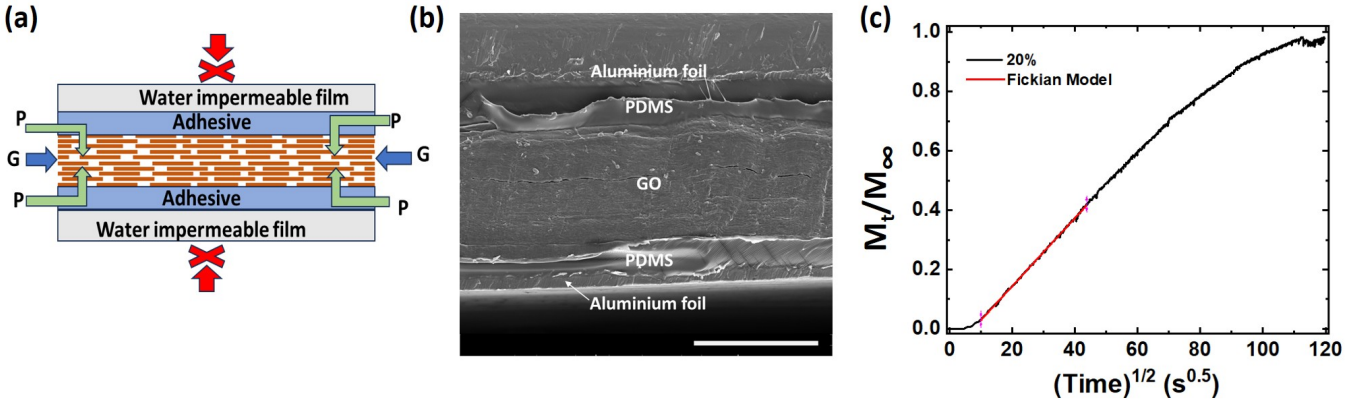

Fig. S11 Schematic illustration of water sorption pathways in the sandwiched geometry, through adhesive to GO (denoted as P) and in-plane diffusion in GO membrane (denoted as G). (b) Cross-sectional FESEM image of a 100 μm-thick sandwiched GO membrane between aluminium foils using PDMS as an adhesive layer. Scale bar: 100 μm. (c) Sorption kinetics of water molecules in GO under an in-plane geometry for a relative humidity (RH) step change from 15% to 20% RH. The initial linear region was fitted using the Fickian diffusion equation to extract the diffusion coefficient. (d) In-plane diffusion coefficient vs. RH% obtained from sorption kinetics for sandwiched geometry. D_{out} is plotted on the right ordinate axis for comparison.

The above results indicate that the total moisture flux contributing to GO membrane sorption through PDMS (P) is approximately an order of magnitude smaller than that through in-plane diffusion in GO (G). This confirms that the contribution of PDMS to the overall sorption kinetics of sandwiched GO is minimal. Therefore, the Fickian equation can be directly implemented to calculate the diffusion coefficient of water within the membrane for the in-plane geometry. Figure S11(c) shows the sorption data fitted with a linear relation based on the Fickian diffusion model for a RH% step from 15% to 20%. The corresponding values of the in-plane diffusion coefficient

Table S8 Simulated sorption time constant for various RH% based on P flux through PDMS into GO. Comparison with experimentally obtained time constants is also shown.

RH%	through PDMS alone (min.)	Experimental (min.)
5%	2150	283
15%	1150	141
20%	680	68
25%	750	45
30%	480	41
45%	395	30

(D_{2D}) as a function of RH are presented in Figure S11(d).

S6.4: Tortuosity

For lamellae-like flakes arrangement, the effective diffusion coefficient due to tortuosity is given by the equation: [18]

$$\frac{D_0}{D_N} = 1 + \frac{d\delta}{s(\delta+b)} + \frac{d^2}{b(\delta+b)}$$

Here, D_0 represents the intrinsic diffusion coefficient in the absence of restrictions, while D_N denotes the effective diffusion coefficient in the presence of impermeable, finite-sized flakes. In this model, $2d$ corresponds to the lateral size of the flakes, $2s$ to the lateral separation between them, and δ and b refer to the flake thickness and vertical spacing, respectively, as depicted in the Fig. S12.

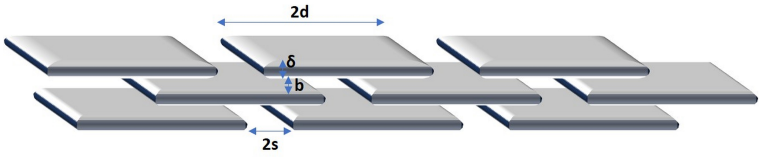

Fig. S12 Schematic for layered lamella structure, offering tortuous pathways in the out-of-plane direction due to the presence of impermeable stacked flakes.

The in-plane diffusion coefficient D_{2D} is taken as D_0 and the out-of-plane coefficient D_{out} as D_N. For $\delta = b \sim 5$ Å and flake size ~ 2 μm, this model predicts a ratio $D_{2D}/D_{out} = 10^7$. This value is 5 orders of magnitude smaller than the value obtained from the diffusion experiments described in the main text.

S7: Out-of-plane permeation for single-side condensation

Table S9 Out-of-plane water vapour permeation rate through GO membrane for single-side condensation (100% RH) or single-side liquid-in-contact on the feed side.

thickness (μm)	Permeation rate (mg/cm^{2}min.)	Normalized permeation rate (μm.mg/cm^{2}min.)	Permeate-side	Feed-side	External Mass Transfer resistance	Reference
0.35 †	2.7	0.95	vacuum	liquid	not mentioned	[19]
~0.2 †	3.2	0.64	vacuum	100% RH	not mentioned	[20]
1	0.25	0.25	< 10 % RH	100% RH	likely high	[21]
1	0.70	0.70	< 10 % RH	100% RH	likely high	[12]
2	0.34	0.68	< 2 % RH	100% RH	high (uncorrected)	This Work
50	0.17	8.65	< 2 % RH	100% RH	high (uncorrected)	This Work
50	0.35	17.5	< 2 % RH	100% RH	corrected	This Work

† Film supported on a filter paper.

S8: Liquid flow through GO membranes

There are inconsistencies in the reported permeation rate of liquid water through the GO membranes [22–25]. In particular, the presence of cracks in the membrane can provide misleading results. Therefore, we first tested the 100% RH saturated GO membrane (0.5 μm thick) for nitrogen gas permeability. A 6-bar pressure was applied, and gas permeation was monitored by counting soap bubble formation. The bubbles of average diameter ~ 2 mm appeared every 30 seconds. These results gave the permeability of N_2 around 0.018 Barrer, consistent with the literature [26] and ensuring the absence of cracks in the membrane. For the liquid water permeation experiments, the permeation cell was filled with liquid water, and a pressure of 5 bar was applied on the liquid column. An initially high permeation flux

was observed, which gradually decreased over time, consistent with previous reports in the literature[22]. After the initial measurement, the pressure was released to ambient conditions, and the membrane was kept immersed in liquid water to allow structural reordering. Subsequent measurements of liquid water permeation were conducted after 15 hours of soaking, and results are presented in the main text.

Table S10 Out-of-plane liquid water permeation rate through GO membrane

thickness (μm)	Permeation rate (L/m^{2}h.bar)	Normalized permeation rate (μm.L/m^{2}h.bar)	Permeate-side	Feed-side	Reference
0.35	0.05	0.018	liquid	liquid	[19]
0.05	3.26	0.166	liquid	liquid	[23]
0.35	0.1 to 0.25	0.035 to 0.09	liquid	liquid	[24]
0.45	0.1	0.04	liquid	liquid	[22]
0.5	0.16	0.08	liquid	liquid	This work

References

[1] J. G. Wijmans and R. W. Baker, *Journal of membrane science*, 1995, **107**, 1–21.

[2] S. Sängerlaub, M. Schmid and K. Müller, *Food packaging and shelf life*, 2018, **17**, 80–84.

[3] J. Crank, *The mathematics of diffusion*, Oxford university press, 1979.

[4] S. Despond, E. Espuche and A. Domard, *Journal of Polymer Science Part B: Polymer Physics*, 2001, **39**, 3114–3127.

[5] J. Barrie, Polymers in a Marine Environment Conference, 1968.

[6] G. Q. Chen, C. A. Scholes, G. G. Qiao and S. E. Kentish, *Journal of Membrane Science*, 2011, **379**, 479–487.

[7] E. Favre, P. Schaetzel, Q. Nguygen, R. Clement and J. Neel, *Journal of Membrane Science*, 1994, **92**, 169–184.

[8] G. A. Ludlam, S. J. Gnaniah, R. Degl'Innocenti, G. Gupta, A. J. Wain and H. Lin, *ACS Sustainable Chemistry & Engineering*, 2024, **12**, 7924–7934.

[9] G. Suresh, A. Pandey and A. Goswami, *Journal of membrane science*, 2006, **284**, 193–197.

[10] P. Majsztrik, A. Bocarsly and J. Benziger, *The Journal of Physical Chemistry B*, 2008, **112**, 16280–16289.

[11] A. Borde, M. Larsson, Y. Odelberg, J. Hagman, P. Löwenhielm and A. Larsson, *Acta biomaterialia*, 2012, **8**, 579–588.

[12] R. Nair, H. Wu, P. N. Jayaram, I. V. Grigorieva and A. Geim, *Science*, 2012, **335**, 442–444.

[13] C. Gustavsson and L. Piculell, *The Journal of Physical Chemistry B*, 2016, **120**, 6778–6790.

[14] A. Thorell and L. Wadsö, *Drying Technology*, 2018, **36**, 332–340.

[15] J.-H. Park and S.-Y. Yoo, *KSME international journal*, 2004, **18**, 1258–1266.

[16] F. Montagnaro, *Energies*, 2024, **17**, 4342.

[17] S. J. Harley, E. A. Glascoe and R. S. Maxwell, *The Journal of Physical Chemistry B*, 2012, **116**, 14183–14190.

[18] E. Cussler, *Journal of Membrane Science*, 1990, **52**, 275–288.

[19] J. Chong, B. Wang and K. Li, *Chemical communications*, 2018, **54**, 2554–2557.

[20] R. Takenaka, N. Moriyama, H. Nagasawa, M. Kanezashi and T. Tsuru, *Membranes*, 2023, **13**, 533.

[21] K.-G. Zhou, K. Vasu, C. Cherian, M. Neek-Amal, J. C. Zhang, H. Ghorbanfekr-Kalashami, K. Huang, O. Marshall, V. Kravets, J. Abraham *et al.*, *Nature*, 2018, **559**, 236–240.

[22] J. Y. Chong, B. Wang, C. Mattevi and K. Li, *Journal of Membrane Science*, 2018, **549**, 385–392.

[23] Y. Han, Z. Xu and C. Gao, *Advanced functional materials*, 2013, **23**, 3693–3700.

[24] V. Saraswat, R. M. Jacobberger, J. S. Ostrander, C. L. Hummell, A. J. Way, J. Wang, M. T. Zanni and M. S. Arnold, *ACS nano*, 2018, **12**, 7855–7865.

[25] Y. Li, J. Zhao, J. Zhang, X. Gong, J. Zhou, N. Zhang and Y. Su, *Nature Communications*, 2025, **16**, 5363.

[26] H. W. Kim, H. W. Yoon, S.-M. Yoon, B. M. Yoo, B. K. Ahn, Y. H. Cho, H. J. Shin, H. Yang, U. Paik, S. Kwon *et al.*, *Science*, 2013, **342**, 91–95.